

Formation of nanoscale Th-coffinite

ARTUR P. DEDITIUS,^{1,*} VÉRONIQUE POINTEAU,^{2,†} JIANG M. ZHANG,² AND RODNEY C. EWING²

¹Institute of Applied Geosciences, Graz University of Technology, Rechbauerstrasse 12, 8010 Graz, Austria

²Department of Earth and Environmental Sciences, University of Michigan, Ann Arbor, Michigan 48109-1005, U.S.A.

ABSTRACT

U-thorite, (Th,U)SiO₄, from Ambohitrova Masindray, Madagascar, was investigated to understand the behavior of Th and U during recrystallization of amorphous radiation-damaged, (Th,U)-orthosilicates. Optical microscopy and electron microprobe analyses reveal two types of U-thorite: (i) large (about 1 cm), orange, amorphous grains with composition: (Th_{0.88±0.02}U_{0.09–0.01}Pb_{0.029±0.002}REE_{0.01±0.001})_{1.00±0.01}Si_{1.00±0.01}; and (ii) green, microcrystalline U-thorite with composition: (Th_{0.76±0.05}U_{0.08±0.01}Ca_{0.07±0.01}Pb_{0.014±0.005}REE_{0.009±0.001})_{0.92±0.07}Si_{1.12±0.06}. Ca-free U-thorite-(i) is enriched in Th, U, and Pb (7.1, 1.2, and 1 wt%, respectively), and depleted in Si (3.0 wt%) compared to U-thorite-(ii). Recrystallization of U-thorite-(i) resulted in fracturing that facilitated migration of mobilized Th and U over a distance of about 300 μm, as evidenced by precipitation of U-thorite-(ii) in the fractures in associated apatite and garnet. Transmission electron microscopy observations and selected-area electron diffraction (SAED) patterns confirm that U-thorite-(i) is amorphous. U-thorite-(ii) forms: (1) single crystals (>1 μm in size) with variable amounts of amorphous material; or (2) randomly oriented, nanocrystalline aggregates (5–10 nm in size). TEM-EDX analyses show that the Th/U ratio in U-thorite-(i) and U-thorite-(ii) is ~6. High-angle annular dark-field scanning TEM (HAADF-STEM) and high-resolution TEM reveal that nanocrystalline Th-coffinite (20–40 nm in size) with Th/U ratio = 0.6, formed during recrystallization of U-thorite-(i). The calculated chemical Th-U-Pb ages of U-thorite-(i) range from 2.1–1.9 Ga and from 1.8–1.6 Ga, whereas U-thorite-(ii) ages range from 1.6–0.5 Ga. The calculated cumulative radiation dose for U-thorite-(i) varies from 1.6–1.8 × 10¹⁸ α-decay events/mg, which is equivalent to 136–152 displacements per atom (dpa), and for U-thorite-(ii) from 3–4.4 × 10¹⁷ (α-decay events/mg) (=27–37 dpa). The cumulative dose for Th-coffinite is 9.8 × 10¹⁷ α-decay events/mg (84 dpa).

Keywords: Thorite, coffinite, nanoparticles, amorphization, recrystallization, Madagascar

INTRODUCTION

Thorite, ThSiO₄, contains significant amounts of U and, therefore, a continuous solid solution with coffinite, USiO₄, has been proposed (e.g., Fuchs and Gebert 1958; Spear 1982; Smits 1989; Förster 2006). U-bearing thorite, uranothorite, forms under higher-temperature magmatic-hydrothermal conditions, whereas coffinite precipitates under low-temperature hydrothermal and/or sedimentary conditions (e.g., Janeczek and Ewing 1992a; Förster et al. 2000). Thus, uranothorite and coffinite can limit migration of tetravalent actinides U and Th under a wide range of Si-rich, reducing conditions that are relevant for proposed geological repositories for spent nuclear fuel (SNF), which is mainly UO₂ (e.g., Janeczek and Ewing 1992b; Finch and Hanchar 2003; Amme et al. 2005; Grambow and Giffaut 2006). However, there are very limited data available on the amorphization, recrystallization, and alteration processes of phases with intermediate chemical compositions (e.g., Lumpkin and Chakoumakos 1988). Most previous research has focused on the variation in the chemical composition of thorite-coffinite

solid solution (e.g., Förster 2006 and references therein) and the amorphization-recrystallization processes of the pure end-members (e.g., Meldrum et al. 1998, 2000; Deditius et al. 2008; Lian et al. 2009). However, Lumpkin and Chakoumakos (1988) and Deditius et al. (2008, 2010) have shown that the chemical composition, structure, and alteration of (Th,U)-orthosilicates shows considerable variation at the nanoscale.

Here we present nanoscale results for the recrystallization of an amorphous (Th,U)-silicate to U- and Th-rich orthosilicates using various electron microscopy techniques and supported by numerous electron microprobe (EMPA) analyses. This study provides new insights into the behavior of U and Th, the stability of U-thorite and Th-coffinite at the nanoscale, and the relation of nanoscale variations in composition to the solid solution of these (Th,U)-orthosilicates.

PREVIOUS STUDIES ON THE THORITE-COFFINITE SOLID-SOLUTION BINARY

Thorite and coffinite are orthosilicates, with general formula ABO₄·nH₂O, where *n* ranges from 0–2; (space group *I4₁/amd*, *Z* = 4). The A-site in thorite and coffinite can be occupied by Th⁴⁺, U^{4+,6+}, Zr⁴⁺, Hf⁴⁺, Y³⁺, REE³⁺, and Ca²⁺, and the B-site can be occupied by Si⁴⁺, P⁵⁺, V⁵⁺, S⁶⁺, F⁻, and OH⁻. Thus, the chemical compositions of thorite and coffinite vary widely due to numer-

* E-mail: deditius@tugraz.at

† Present address: CEA/Cadarache DTN/STRI/LHC 13108 Saint Paul lez Durance Cedex, France.

ous iso- and heterovalent substitutions. Such substitutions have been extensively reviewed in the literature (e.g., Spear 1982; Smits 1989; Janeczek and Ewing 1992a; Burns 1999; Finch and Hanchar 2003; Förster 2006; Breiter et al. 2009; Deditius et al. 2009). Frequently reported chemical substitutions include: (1) $\text{Th}^{4+} \leftrightarrow \text{U}^{4+} \leftrightarrow \text{Zr}^{4+}$; (2) xenotime-type: $\text{P}^{5+} + (\text{Y,REE})^{3+} \leftrightarrow \text{Si}^{4+} + (\text{Th,U})^{4+}$; (3) brabantite-type: $\text{Ca}^{2+} + 2\text{P}^{5+} + (\text{U,Th})^{4+} \leftrightarrow 2\text{Si}^{4+} + 2\text{Zr}^{4+}$; (4) ningyuite-type: $0.8\text{P} + 2\text{Ca}^{2+} + 0.2(\square)^{\text{IV}} \leftrightarrow \text{Si}^{4+} + (\text{Th,U})^{4+}$; and (5) $4(\text{OH})^- \leftrightarrow \text{SiO}_4^{4-}$. The substitution of U^{4+} for Th^{4+} is facilitated by similar charge and ionic radius [0.100 nm and 0.105 nm for eightfold coordination, respectively (Shannon 1976)]. Infrared (IR) studies of thorite have revealed that H_2O -species dominate in the thorite structure with lower amounts of OH, without specific structural position (Lumpkin and Chakoumakos 1988). Fuchs and Hoekstra (1959) assigned the observed OH vibrations in coffinite to the presence of hydrated SiO_2 rather than to the hydroxyl-substitution. In contrast, Kamineneni and Lemire (1991) proposed that hydrothermal thorite from Atikokan (Canada) contains structural water.

EMPA of (Th,U)-orthosilicates from Witwatersrand (Smits 1989) revealed a maximum of 36 mol% of USiO_4 in thorite and 19 mol% of ThSiO_4 in coffinite. Based on X-ray diffraction (XRD) analyses, Smits (1989) reported that U-thorite is metamict, and Th-coffinite is crystalline. Similar concentrations of UO_2 in thorite were found by Pointer et al. (1988); i.e., <35 mol% of USiO_4 . However, there are important differences between thorite and coffinite. Thorite often contains between 0–10 mol% of USiO_4 , and the crystals are tens of micrometers in size (e.g., Förster 2006). Usually, concentrations of Th in coffinite are typically below the detection limit of the electron microprobe, and its grains are less than 10 μm in size (Hansley and Fitzpatrick 1989; Deditius et al. 2008). Thorite precipitates at temperatures between 200–400 °C, whereas coffinite does so at $T < 130$ °C (e.g., Janeczek and Ewing 1992a; Förster et al. 2000; Johan and Johan 2005). In addition, coffinite is often reported to be an alteration product of uraninite under Si-rich, low-temperature, reducing conditions, whereas thorite precipitates directly from magmatic-hydrothermal fluids and rarely replaces thorianite, ThO_2 (e.g., Spear 1982; Janeczek and Ewing 1992a; Janeczek 1999; Förster et al. 2000; Förster 2006; Deditius et al. 2008, 2010). The only transmission electron microscopy (TEM) study of U-thorite (with 0.3 mol% of UO_2 , from the Harding pegmatite in New Mexico) revealed a heterogeneous distribution of amorphous and randomly oriented crystalline domains 50 nm (Lumpkin and Chakoumakos 1988). Additional high-resolution transmission electron microscopy (HRTEM) observations of coarse-grained coffinite (from the Grants uranium region in New Mexico) have shown single crystals without an amorphous fraction (Deditius et al. 2008) in contrast to significant amorphization of P-coffinite from Bangombé, Gabon (Deditius et al. 2009).

Synthesis of thorite is relatively straightforward, but there are only few successful syntheses of coffinite and/or uranorthite (Fuchs and Gebert 1958; Mumpton and Roy 1961; Pointeau et al. 2009). Fuchs and Gebert (1958) synthesized thorite-coffinite solid solution with U/Th ratios: 25/75, 50/50, 75/25. However, Mumpton and Roy (1961) obtained thorite with <30 mol% of coffinite end-member. Pointeau et al. (2009) have synthesized coffinite, identified by XRD and TEM, with minor nanocrystal-

line UO_2 , <5 nm, and some amorphous phase present. Computational analysis of the thorite-coffinite solid solutions showed that a mixture of UO_2 and SiO_2 is more stable than USiO_4 under low-temperature conditions, in contrast to calculations for thorite (Ferriss et al. 2010).

Natural thorite and coffinite are often reported to be completely or partly amorphous due to radiation damage from U and Th α -decay (Janeczek and Ewing 1992a; Förster et al. 2000; Deditius et al. 2009). The persistence of the metamict state in thorite, zircon, hafnon, and xenotime is due to the high-activation energies (3–3.6 eV) for recrystallization as determined by ion beam irradiation experiments (Meldrum et al. 1998). Recently, Lian et al. (2009) showed that the activation energy for recrystallization of coffinite is much lower and equals 0.28 eV. Also, the critical temperature for amorphization of coffinite is 608 K, whereas it is 1100 K for thorite. The two-phase region for coffinite (UO_2+SiO_2) is as low as 673 K, whereas thorite ($\text{ThO}_2+\text{SiO}_2$) is >2250 K (Meldrum et al. 1998; Lian et al. 2009).

SAMPLES AND METHODS

The analyzed samples of U-thorite, no. 5857, come from a pegmatite from Ambohijatrova, Masindray, Madagascar, which were provided by courtesy of Ecole des Mines de Paris, France. Samples were first examined in polished thin and thick sections by optical and scanning electron microscopy (SEM, Hitachi S3200N equipped with energy dispersive X-ray spectrometry, EDS). The chemical composition of U-thorite was quantitatively determined by EMPA (Cameca SX100). The accelerating voltage and beam current were 20 kV and 40 nA, respectively, and the beam diameter was 1 μm . The counting times on the peak were 60 s and a half of that time on both sides of the peak. The PAP correction procedure was used to calculate the analyses. The standards used for calibration and detection limits (in ppm, given in parentheses) were: albite for $\text{AlK}\alpha$ (84 ppm) and $\text{NaK}\alpha$ (195); CaTiO_3 for $\text{CaK}\alpha$ (185) and $\text{TiK}\alpha$ (194); YPO_4 and ErPO_4 for $\text{PK}\alpha$ (174) and $\text{YL}\alpha$ (439); andradite for $\text{SiK}\alpha$ (134) and $\text{FeK}\alpha$ (172); MgO for $\text{MgK}\alpha$ (152); synthetic KTaO_3 for $\text{KK}\alpha$ (139); BaSO_4 for $\text{SK}\alpha$ (144); cerussite for $\text{PbM}\beta$ (893); zircon (ZrSiO_4) for $\text{ZrL}\alpha$ (142); synthetic UO_2 for $\text{UM}\beta$ (924); ThSiO_4 for $\text{ThM}\alpha$ (755); LaPO_4 for $\text{LaL}\alpha$ (457); CePO_4 for $\text{CeL}\alpha$ (442); PrPO_4 for $\text{PrL}\beta$ (644); NdPO_4 for $\text{NdL}\alpha$ (314); SmPO_4 for $\text{SmL}\beta$ (508); GdPO_4 for $\text{GdL}\beta$ (571); DyPO_4 for $\text{DyL}\beta$ (592); ErPO_4 for $\text{ErL}\beta$ (767).

HRTEM, analytical electron microscopy (AEM), and high-angle annular dark-field scanning transmission electron microscopy (HAADF-STEM) were conducted using a JEOL JEM2010F. The spherical coefficient C_s is 1.0 mm. In STEM mode, the probe size was 1.0 nm and the collection angle of the HAADF detector was 50–110 mrad. The size of the condenser aperture was 20 μm .

RESULTS

Occurrence of U-thorite

U-thorite forms as large crystals (about 1 cm) associated with apatite-(CaF), garnet, zircon, titanite, and biotite. The U-thorite consists of two different phases: optically isotropic, orange U-thorite-(i); and green U-thorite-(ii), which consists of polycrystalline aggregates that form a worm-like texture that penetrates the core and rims of U-thorite-(i) (Figs. 1a–1c). This texture suggests replacement and/or recrystallization of U-thorite-(i) by crystalline U-thorite-(ii). Backscattered electron (BSE) images reveal heterogeneous contrast and colloform textures of U-thorite-(ii) caused by variation in Th-content (Fig. 1d). Fracturing of U-thorite-(ii) is caused by the accompanying volume change between amorphous U-thorite-(i) and the recrystallized product. U-thorite grains are surrounded by a 10–30 μm thick layer of fine-grained biotite (Fig. 1e). Amorphous U-thorite-(i) is characterized by brighter contrast in BSE images than U-thorite-(ii) (Fig. 1d). In addition, grains of U-thorite-(ii), 5 μm in size,

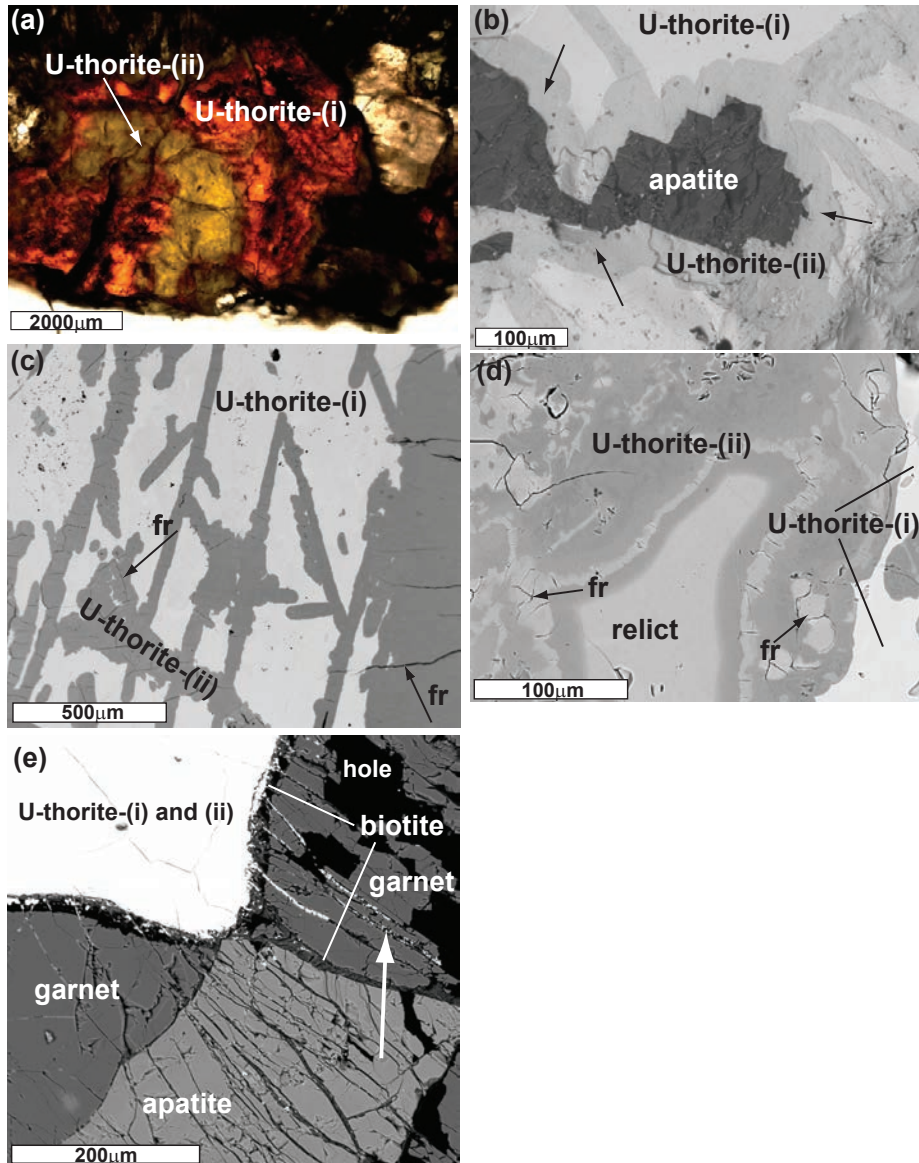
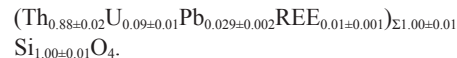


FIGURE 1. Optical and BSE images of U-thorite and associated apatite and garnet. (a) Transmitted light microscope image of amorphous, orange U-thorite-(i); and crystalline, green U-thorite-(ii). (b–c) Worm-like textures developed during alteration of amorphous to crystalline U-thorite. Note the alteration rim of crystalline U-thorite-(ii) (lower BSE contrast; black arrows) separating U-thorite-(i) from apatite. (d) Relict of U-thorite-(i). Note the inhomogeneous BSE contrast and collomorphic texture of U-thorite-(ii) and fracturing (fr) (images, c and d). (e) Formation of secondary U-thorite-(ii) in fractures within garnet and apatite (white arrow). U-thorite is mantled by biotite. (Color online.)

occur along fractures in the associated apatite-(CaF) and garnet (Fig. 1e). No uraninite and/or thorianite, ThO_2 , were observed in the amorphous or crystalline U-thorite.

Chemical composition of U-thorite

The chemical compositions of U-thorite-(i) and U-thorite-(ii) are significantly different (Tables 1 and 2). The major components of the U-thorite-(i) are ThO_2 (68.43–76.53 wt%), SiO_2 (18.01–19.23 wt%), and UO_2 (6.73–9.78 wt%). The chemical composition of the amorphous U-thorite-(i) varies over a relatively narrow range (i.e., within a standard deviation)



A characteristic feature of U-thorite-(i) is the relatively high concentration of PbO that varies over a fairly narrow range from 1.83–2.17 wt%; and a lack of CaO compared to U-thorite-(ii) (0.96–1.46 wt% CaO). The SO_3 content varies from 0.09–0.33 wt%. The total concentration of (Y,Ce,Nd,Gd,Er) $_2\text{O}_3$ is below 0.66 wt%. The concentrations of Na_2O , Al_2O_3 , FeO, K_2O , ZrO_2 , and TiO_2 are below 0.2 wt%, and those of P_2O_5 , La_2O_3 , Pr_2O_3 , Sm_2O_3 , and Dy_2O_3 are below detection limits (bdl). The aver-

TABLE 1. Representative analyses of U-thorite-(i)

Oxides	1	2	3	4	5	6	7	8	9	10
Na ₂ O	0.03	0.09	0.11	0.03	0.04	n.a.	n.a.	n.a.	n.a.	n.a.
K ₂ O	0.03	0.03	0.03	0.04	0.04	n.a.	n.a.	n.a.	n.a.	n.a.
SiO ₂	19.04	18.90	18.97	19.01	18.89	18.71	18.60	18.53	18.18	18.41
SO ₃	0.11	0.09	0.16	0.33	0.09	n.a.	n.a.	n.a.	n.a.	n.a.
TiO ₂	0.05	0.03	0.04	0.04	0.04	n.a.	n.a.	n.a.	n.a.	n.a.
ZrO ₂	bdl	0.03	0.05	0.04	0.04	n.a.	n.a.	n.a.	n.a.	n.a.
FeO	0.02	0.02	0.02	0.02	bdl	n.a.	n.a.	n.a.	n.a.	n.a.
Y ₂ O ₃	n.a.	n.a.	n.a.	n.a.	n.a.	0.06	0.14	0.07	0.13	0.08
Ce ₂ O ₃	n.a.	n.a.	n.a.	n.a.	n.a.	0.12	0.15	0.11	0.15	0.13
Nd ₂ O ₃	n.a.	n.a.	n.a.	n.a.	n.a.	0.12	0.21	0.15	0.19	0.15
Gd ₂ O ₃	n.a.	n.a.	n.a.	n.a.	n.a.	bdl	bdl	0.05	0.05	0.04
Er ₂ O ₃	n.a.	n.a.	n.a.	n.a.	n.a.	0.12	0.13	0.12	0.11	0.11
PbO	1.93	2.02	2.00	1.90	1.83	2.17	2.07	1.99	1.99	1.99
UO ₂	7.01	8.83	8.74	7.05	6.86	9.45	7.68	7.48	7.66	7.80
ThO ₂	71.31	69.66	69.96	71.60	72.81	69.63	71.14	71.11	70.16	71.73
Total	99.53	99.70	100.08	100.05	100.65	100.41	100.12	99.61	98.62	100.44
Na ⁺	0.002	0.005	0.005	0.006	0.001	n.a.	n.a.	n.a.	n.a.	n.a.
K ⁺	0.001	0.001	0.001	0.001	0.001	n.a.	n.a.	n.a.	n.a.	n.a.
Si ⁴⁺	1.022	1.016	1.015	1.008	1.002	1.011	1.006	1.007	1.001	0.998
S ⁶⁺	0.039	0.033	0.058	0.068	0.041	n.a.	n.a.	n.a.	n.a.	n.a.
Ti ⁴⁺	0.002	0.001	0.002	0.002	0.001	n.a.	n.a.	n.a.	n.a.	n.a.
Zr ⁴⁺	bdl	0.001	0.001	0.001	0.001	n.a.	n.a.	n.a.	n.a.	n.a.
Fe ²⁺	0.001	0.001	0.001	bdl	bdl	n.a.	n.a.	n.a.	n.a.	n.a.
Y ³⁺	n.a.	n.a.	n.a.	n.a.	n.a.	0.003	0.004	0.002	0.004	0.002
Ce ³⁺	n.a.	n.a.	n.a.	n.a.	n.a.	0.003	0.003	0.002	0.003	0.002
Nd ³⁺	n.a.	n.a.	n.a.	n.a.	n.a.	0.003	0.004	0.003	0.004	0.003
Gd ³⁺	n.a.	n.a.	n.a.	n.a.	n.a.	0.001	0.001	0.001	0.001	0.001
Er ³⁺	n.a.	n.a.	n.a.	n.a.	n.a.	0.002	0.002	0.002	0.002	0.002
Pb ²⁺	0.028	0.029	0.029	0.028	0.027	0.029	0.030	0.029	0.029	0.029
U ⁴⁺	0.084	0.106	0.104	0.104	0.081	0.092	0.092	0.090	0.094	0.094
Th ⁴⁺	0.870	0.853	0.852	0.857	0.893	0.875	0.876	0.879	0.879	0.885
Total	2.049	2.046	2.068	2.075	2.048	2.018	2.018	2.015	2.017	2.016

* MgO, Al₂O₃, CaO, La₂O₃, Pr₂O₃, Sm₂O₃, P₂O₅, Dy₂O₃ – not detected.

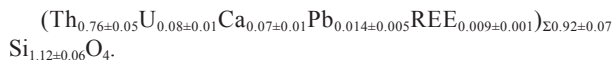
TABLE 2. Representative analyses of U-thorite-(ii)

Oxides	1	2	3	4	5	6	7	8	9	10
K ₂ O	0.04	0.03	0.03	0.02	0.03	n.a.	n.a.	n.a.	n.a.	n.a.
MgO	0.03	0.04	bdl	0.05	0.03	n.a.	n.a.	n.a.	n.a.	n.a.
Al ₂ O ₃	bdl	0.38	bdl	0.40	bdl	n.a.	n.a.	n.a.	n.a.	n.a.
SiO ₂	20.84	24.66	20.79	25.39	19.96	24.50	22.23	19.38	24.00	23.46
SO ₃	0.04	0.05	0.05	0.02	0.05	n.a.	n.a.	n.a.	n.a.	n.a.
CaO	1.35	1.06	1.46	0.96	1.26	1.06	1.29	1.32	1.17	1.43
TiO ₂	0.02	0.03	0.03	0.03	0.02	n.a.	n.a.	n.a.	n.a.	n.a.
ZrO ₂	0.03	0.02	bdl	bdl	0.04	n.a.	n.a.	n.a.	n.a.	n.a.
FeO	0.02	0.02	bdl	0.03	bdl	n.a.	n.a.	n.a.	n.a.	n.a.
Y ₂ O ₃	n.a.	n.a.	n.a.	n.a.	n.a.	0.06	0.07	0.09	0.08	0.05
Ce ₂ O ₃	n.a.	n.a.	n.a.	n.a.	n.a.	0.10	0.10	0.11	0.11	0.07
Nd ₂ O ₃	n.a.	n.a.	n.a.	n.a.	n.a.	0.13	0.13	0.15	0.14	0.11
Er ₂ O ₃	n.a.	n.a.	n.a.	n.a.	n.a.	0.13	0.15	0.15	0.12	0.08
PbO	1.38	0.58	1.32	0.62	1.40	0.70	0.68	1.29	0.70	0.71
UO ₂	6.48	7.41	6.78	6.33	6.55	5.24	6.36	7.44	5.76	8.67
ThO ₂	65.09	61.98	69.73	61.58	70.22	64.49	65.63	65.21	65.73	62.80
Total	95.32	96.26	100.19	95.44	99.56	96.38	96.64	95.14	97.87	97.38
K ⁺	0.001	0.001	0.001	0.002	0.001	n.a.	n.a.	n.a.	n.a.	n.a.
Mg ²⁺	0.002	0.003	bdl	0.002	0.002	n.a.	n.a.	n.a.	n.a.	n.a.
Al ³⁺	bdl	0.011	bdl	bdl	bdl	n.a.	n.a.	n.a.	n.a.	n.a.
Si ⁴⁺	1.093	1.193	1.051	1.073	1.040	1.191	1.126	1.050	1.168	1.154
S ⁶⁺	0.014	0.015	0.017	0.009	0.017	n.a.	n.a.	n.a.	n.a.	n.a.
Ca ²⁺	0.076	0.055	0.080	0.070	0.070	0.055	0.070	0.077	0.061	0.075
Ti ⁴⁺	0.001	0.001	0.001	0.002	0.001	n.a.	n.a.	n.a.	n.a.	n.a.
Zr ⁴⁺	0.001	0.001	bdl	0.001	0.001	n.a.	n.a.	n.a.	n.a.	n.a.
Fe ²⁺	0.001	0.001	bdl	0.001	bdl	n.a.	n.a.	n.a.	n.a.	n.a.
Y ³⁺	n.a.	n.a.	n.a.	n.a.	n.a.	0.001	0.002	0.003	0.002	0.001
Ce ³⁺	n.a.	n.a.	n.a.	n.a.	n.a.	0.002	0.002	0.002	0.002	0.001
Nd ³⁺	n.a.	n.a.	n.a.	n.a.	n.a.	0.002	0.002	0.003	0.002	0.002
Er ³⁺	n.a.	n.a.	n.a.	n.a.	n.a.	0.002	0.002	0.003	0.002	0.001
Pb ²⁺	0.020	0.008	0.019	0.018	0.020	0.009	0.009	0.019	0.009	0.009
U ⁴⁺	0.076	0.080	0.078	0.078	0.076	0.057	0.072	0.090	0.073	0.095
Th ⁴⁺	0.777	0.682	0.815	0.798	0.832	0.713	0.756	0.804	0.728	0.703
Total	2.062	2.051	2.062	2.054	2.060	2.032	2.041	2.051	2.047	2.041

* Na₂O, La₂O₃, Pr₂O₃, Sm₂O₃, P₂O₅, Gd₂O₃, Dy₂O₃ – not detected.

age analytical total of U-thorite-(i) is 100.63 ± 1.93 wt%, which indicates the absence of or very low H₂O or OH-species contents in U-thorite-(i).

The chemical composition of U-thorite-(ii) is more variable than that of U-thorite-(i). On average, U-thorite-(ii) contains lower ThO₂ (59.79–70.22 wt%) and UO₂ (4.45–9.01 wt%), and higher SiO₂ (19.37–26.91 wt%) compared to U-thorite-(i) (Table 2). The chemical formula of U-thorite-(ii) is



The chemical formula of U-thorite-(ii) deviates from the theoretical Th/Si ratio of 1/1, due to a loss of Th from the A-site and an excess of Si in the B-site. U-thorite-(ii) contains lower concentrations of PbO (0.49–1.46 wt%) than U-thorite-(i). The Al₂O₃ content is variable (from bdl to 0.52 wt%) and is correlative to depletion of ThO₂ and an increase in SiO₂. This is suggestive of the presence of aluminosilicate inclusions. U-thorite-(ii) contains less than 0.56 wt% of (Y,Ce,Nd,Gd,Er)₂O₃. The concentrations of Na₂O, FeO, K₂O, ZrO₂, and TiO₂ are below 0.1 wt%. The average analytical total of U-thorite-(ii) is 96.04 ± 2.16 wt%, which suggests significant amounts of H₂O and/or OH⁻ species (Table 2), as reported for U-thorite from other localities (e.g., Spear 1982; Lumpkin and Chakoumakos 1988).

Elemental maps show the relative concentrations of Th, Ca, Pb, and Si within associated U-thorite-(i) and -(ii) (Fig. 2a). Higher concentrations of Ca and Si correlate inversely with Th and Pb. The EMPA analyses and maps are evidence for the loss of Th, U, and Pb during recrystallization of U-thorite-(i) into U-thorite-(ii) and suggest that the alteration of U-thorite-(i) was caused by a Ca-rich fluid (Figs. 2b and 2c). Sulfur accumulates in U-thorite-(i) (Fig. 2d). There is a weak ($R^2 = 0.28$) positive correlation between Ca and U in U-thorite-(ii) (Fig. 2e). A plot of U-thorite-(ii) analyses on the ternary diagram after Mumpton and Roy (1961) shows that the data is distributed along the tie line toward the H₂O corner (Fig. 2f). Therefore, it appears that the H₂O is the dominant species in the U-thorite-(ii) structure as compared with OH⁻-species, although the presence of OH⁻ cannot be ruled out.

Structure of U-thorite and calculated cumulative α -decay dose

HRTEM observations and selected area diffraction (SAED) patterns show that U-thorite-(i) is completely amorphous; no crystalline areas are present in the amorphous matrix (Fig. 3a). The HAADF-STEM studies reveal that U-thorite-(ii) is associated with aggregates of nanoparticulate Th-coffinite (Fig. 3b). U-thorite-(ii) consists of: (1) randomly oriented nanoparticles (NPs) (4–5 nm in size); and (2) single crystals of U-thorite (>1 μm in size). Both contain various amounts of amorphous material (Figs. 3c–3d). The areas that show nanoparticulate U-thorite-(ii) and an amorphous fraction are characterized by a diffuse SAE ring diffraction pattern (Fig. 3d). The fast Fourier transform (FFT) of the HRTEM image of nanoparticulate U-thorite shows tetragonal symmetry of ThSiO₄ (Fig. 3d). Th-coffinite occurs as aggregates of crystalline NPs (5 to 50 nm in size) (Fig. 3e). Some of the Th-coffinite NPs assemble by means of epitaxial growth. However, random orientations are also observed (Fig. 3f). The

TEM-EDX analyses of U-thorite-(i) and -(ii), and Th-coffinite show that the Th/U ratios are about 6 and 0.6, respectively.

The amorphization of U-thorite results from α -decay events. Calculations of cumulative dose were conducted using the formula given by Ewing et al. (2000), which involves U- and Th-content and the estimated age of the analyzed samples. Although the age of the analyzed U-thorite is unknown, we calculated the Th-U-Pb chemical ages using Cameron-Shiman's equation quoted by Bowles (1990). Three distinct groups of ages were identified in the analyzed samples: (1) 2.1–1.9 Ga (2.0 ± 0.07), (2) 1.8–1.6 Ga (1.7 ± 0.05) for U-thorite-(i), and (3) 1.6–0.5 Ga for U-thorite-(ii). Age differences of U-thorite-(i) are due to local variations of Th, U, and Pb concentrations that were undetectable in the BSE images; i.e., no zoning was observed (Figs. 1b–1e). The large variation in U-thorite-(ii) ages reflect its textural heterogeneity and loss of Th and Pb (Figs. 1 and 2), which is often reported for recrystallized orthosilicates (e.g., Geisler et al. 2007). An age of 2.0 Ga was assumed for the calculation of cumulative doses for U-thorite-(i). The calculated chemical age of U-thorite-(ii) varies from 1.6–0.5 Ga, which indicates significant alteration. We used an age of 570 Ma, which is reported as the age of late, regional scale magmatic-hydrothermal activity that affected Madagascar (e.g., Paquette and Nédélec 1998).

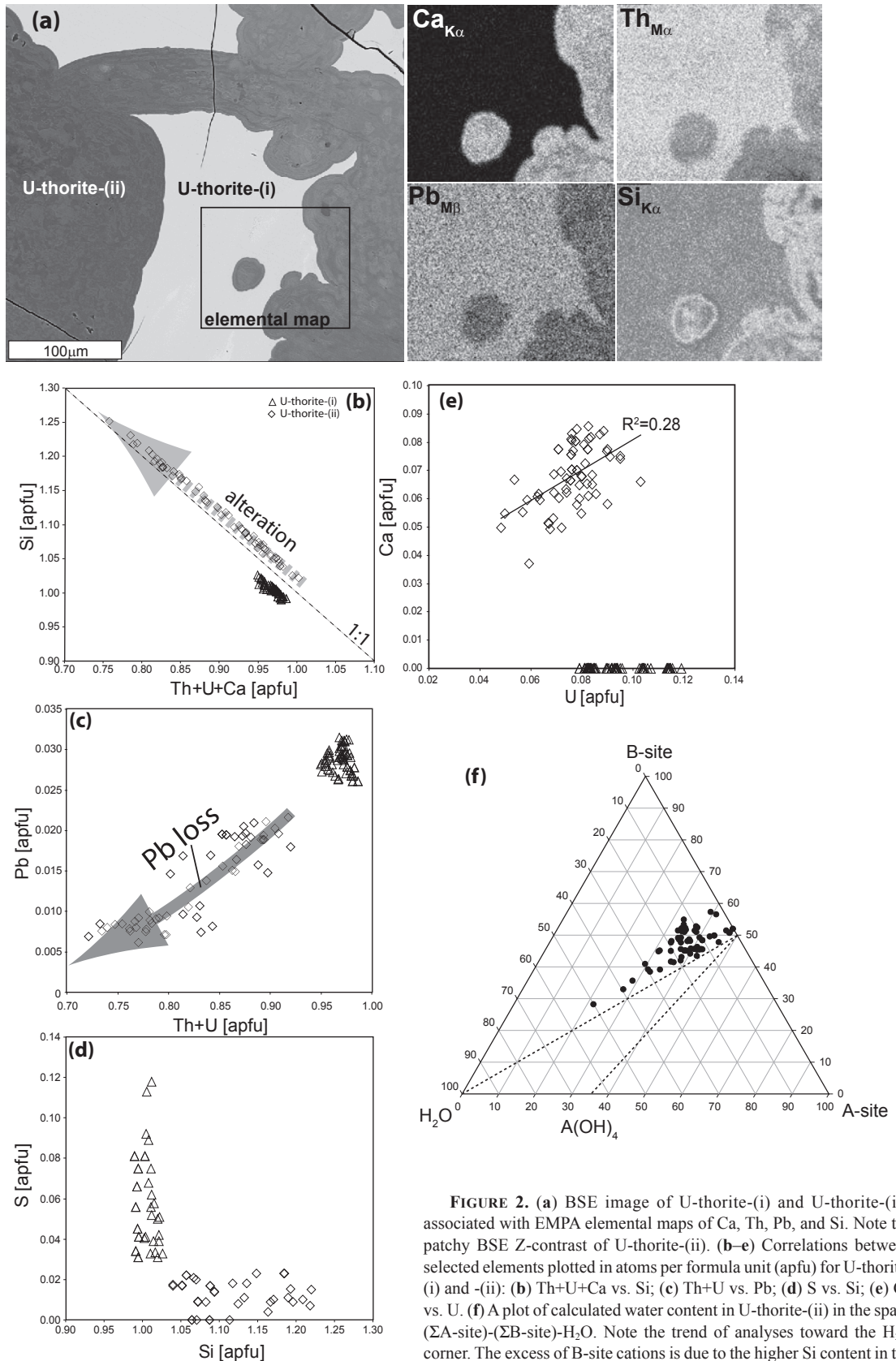
The cumulative dose of the U-thorite-(i) varies between $1.6\text{--}1.8 \times 10^{18}$ α -decay events, which is equivalent to 135–150 displacements per atom (dpa), whereas the U-thorite-(ii) accumulated dose ranges from $3\text{--}4.4 \times 10^{17}$ α -decay events which is equivalent to 27–37 dpa. The calculated doses are much higher than those reported for thorite (0.16 dpa, room temperature to 500 K), or other orthosilicates, which vary from 0.2–0.6 dpa (e.g., Meldrum et al. 1998). The age of Th-coffinite, (U_{0.625}Th_{0.375})SiO₄ (formula calculated based on a Th/U ratio of 0.6), is unknown. However, its secondary origin suggests that it formed synchronously with U-thorite-(ii) ~0.5 Ga ago. The calculated cumulative dose is 9.8×10^{17} α -decay events, which is 84 dpa; which is about 3 times higher than that of U-thorite-(ii).

DISCUSSION

Thorite-coffinite solid solution

EMPA and XRD analyses of natural samples indicate up to 36 mol% of USiO₄ in thorite and up to 19 mol% of ThSiO₄ in coffinite (Pointer et al. 1988; Smits 1989; Förster 2006). One synthesis experiment suggests that there is a continuous solid solution between thorite and coffinite (Fuchs and Gebert 1958). However, the extent of solid solution is unknown due to the difficulty in the synthesis of intermediate and U-rich members of the thorite-coffinite series (Mumpton and Roy 1961; <35 mol% of USiO₄) and lack of nanostructural data of natural uranorthorite that would confirm the occurrence of a single structure with an intermediate composition.

The analyzed U-thorite-(i) and U-thorite-(ii) from Madagascar contain up to 9.8 wt% of UO₂, which is 12 mol% of USiO₄ end-member (Tables 1 and 2). This amount of U is among the most commonly reported for thorite (e.g., Förster 2006 and references therein). Figure 4 shows a diagram of the occupancy for A and B sites in U-thorite-(i) and -(ii), and published analyses. A/B ratios in U-thorite-(i) vary from 0.93–1.0 and cluster close to the theoretical ratio of 1/1 similar to analyses of U-thorite



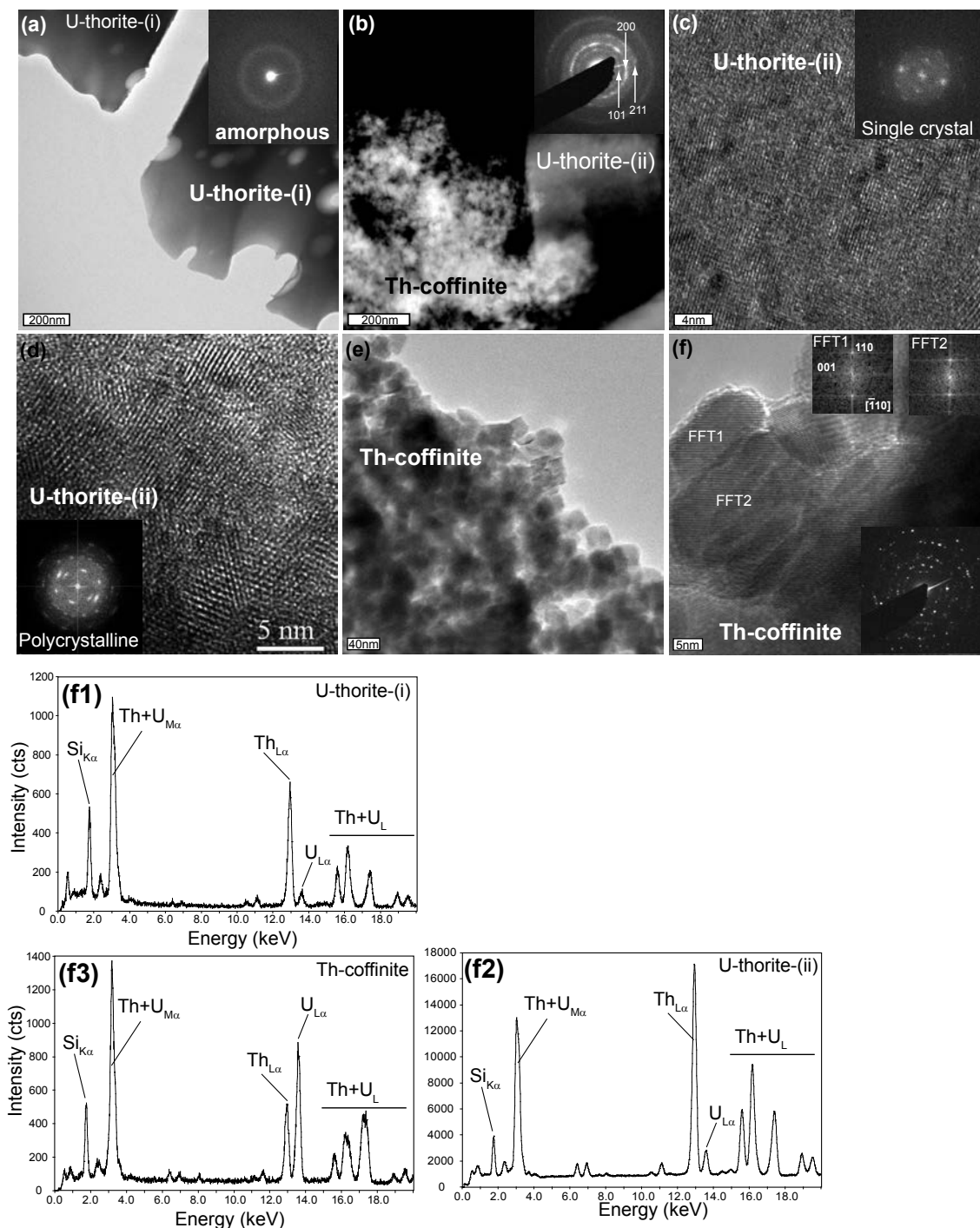


FIGURE 3. HRTEM and HAADF-STEM images and TEM-EDX analyses of U-thorite-(i), U-thorite-(ii), and Th-coffinite. (a) Low-magnification image of U-thorite-(i) associated with diffused SAED pattern that indicates a metamict state; (b) HAADF-STEM image of the associated Th-coffinite and crystalline U-thorite-(ii); the diffuse SAE ring diffraction pattern of U-thorite-(ii) documents the aggregate of randomly oriented nanoparticles. (c) HRTEM image of U-thorite-(ii) associated with fast Fourier transform (FFT) diffraction pattern of the HR-image; disk-like shape of the diffraction maxima suggests a small angle misorientation of the crystalline domains; (d) HRTEM image of randomly oriented NPs of U-thorite-(ii) associated with FFT diffraction pattern; note the discoidal shapes of the diffraction maxima that reflect misorientation of the individual NPs. (e) The aggregate of nanoparticulate Th-coffinite; (f) HRTEM image of Th-coffinite NPs. The SAE ring diffraction pattern shows misorientation of single crystals of Th-coffinite in the aggregate. The FFT of the HRTEM image (FFT1 and FFT2) document the similar orientation of the associated NPs of Th-coffinite; (f1–f3) TEM-EDX spectra of (Th,U)-silicates. Note the relatively similar Th/U ratios between crystalline and amorphous U-thorite (f1–f2) (Th and $U_{L\alpha}$ lines) and the higher concentration of U than Th in Th-coffinite.

from New Zealand (Förster et al. 2000). However, analyses of U-thorite-(ii), ranging from 0.61–0.98 A/B ratio, plot along the theoretical 1/1 line. This shift toward higher concentrations of cations in the B-site is due to an increase in concentration of Si, which is probably located within the amorphous areas of U-thorite-(ii) (Figs. 3c–3d). Similarly, higher cation totals were found in U-thorite from the Harding pegmatite in New Mexico (Lumpkin and Chakoumakos 1988) and Atikokan in Canada (Kamineneni and Lemire 1991). An excess of A-site cations, possibly caused by inclusions of uraninite in thorite, was reported by Johan and Johan (2005), Abd El-Naby (2009), and Pointer et al. (1988). An excess of A-site cations was also noted in coffinite and thorite from Ririwai (Fig. 4). This is reportedly due to high concentrations of Y_2O_3 (up to 12.3 wt%) and relatively small concentrations of P (generally <2.8 wt%) that cause a charge imbalance (Pointer et al. 1988). To balance the charge, Pointer et al. (1988) suggested partial oxidation of U^{4+} to U^{6+} by means of the $2Y^{3+} + U^{6+} = 3U^{4+}$ substitution and/or incorporation of hydroxyls into the tetrahedral position. In contrast, the reported analyses of U-thorite from Madagascar reveal that it contains relatively small concentrations of Y+REE (<0.66 wt%), and no detectable P (Tables 1 and 2). Consequently, all substitutions involving P, such as the xenotime-, brabantite-, and ningyosite-type substitutions can be discounted. U-thorite-(ii) contains significant concentrations of Ca^{2+} (Table 2) that were incorporated into U-thorite-(ii) during recrystallization of U-thorite-(i) (Fig. 2b). Due to the lack of P in U-thorite, the large Ca^{2+} cation (ionic radius 0.112 nm in eightfold coordination; Shannon 1976) can be incorporated into U-thorite-(ii) by means of the following

substitutions: (1) $(REE+Y)^{3+} + Ca^{2+} \leftrightarrow 2(U,Th)^{4+}$ and (2) $Ca^{2+} + U^{6+} \leftrightarrow 2U^{4+}$ (Pointer et al. 1988; Janeczek 1991; Förster 2006). Relatively low concentrations of Y+REE (Table 2) suggest limited operation of substitution (1). The slightly positive correlation between U and Ca ($R^2 = 0.28$) (Fig. 2e), suggests some oxidation of U to hexavalent species by means of substitution (2) in recrystallized U-thorite-(ii). However, U^{6+} -species may also accumulate in the amorphous areas of U-thorite-(ii) (Figs. 3c–3d), as documented by Farges and Calas (1991) in metamict U-thorite. Calcium in U-thorite-(ii) may also concentrate in amorphous areas (Fig. 3c), which was suggested by Breiter et al. (2009) and Žáček et al. (2009).

Divalent Pb (ionic radius 0.129 nm in eightfold coordination; Shannon 1976) is incompatible with the thorite and coffinite structures and often precipitates as microcrystalline galena or clausthalite (PbSe) (e.g., Janeczek and Ewing 1992b; Deditius et al. 2008). However, no galena or other Pb-bearing phases have been observed in U-thorite-(i) and -(ii), or in the associated Th-coffinite. This suggests that Pb probably accumulated in the amorphous areas of U-thorite (Fig. 3).

A review of the EMP analyses of thorite, coffinite, and uranorthite is presented in Figures 5 and 6. Figure 5 displays variation of thorite-coffinite chemical compositions in the space: (Th+Zr)-U-(Y+REE) for A-site cations; and (S-Si-P) for B-site cations (Figs. 5a and 5b).

Considering A-site compositions, thorite and coffinite incorporate up to about 30 mol% of xenotime end-member (Fig. 5a). Thorite forms a mixed solid solution with xenotime (to 14.2 mol%) and coffinite (to 35.6 mol%) (Žáček et al. 2009). Coffinite

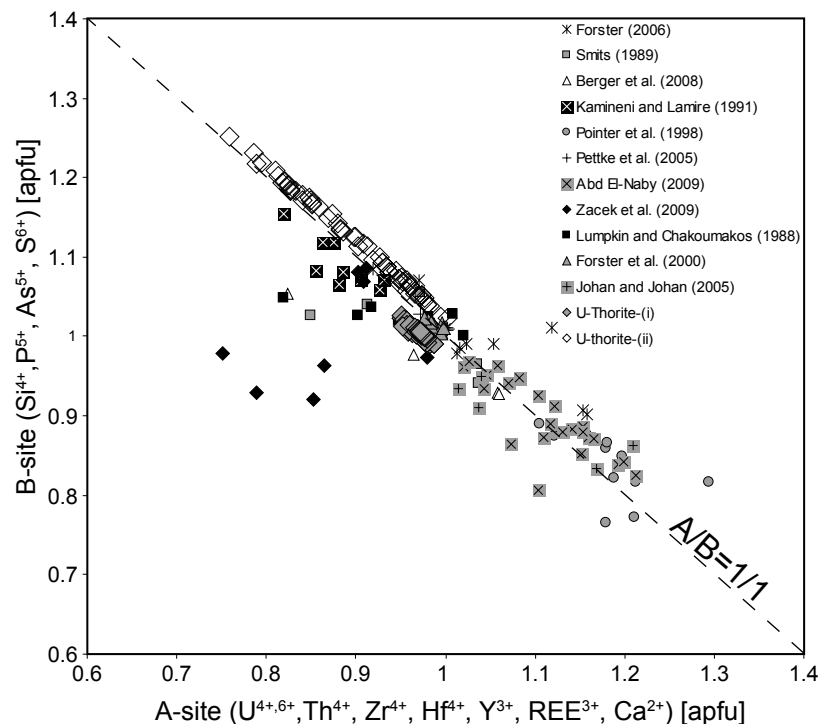


FIGURE 4. A plot of A-site vs. B-site occupancy in U-thorite-(i) and U-thorite-(ii), along with published analyses of (Th,U)-orthosilicates. Note the proximity of analytical points of U-thorite-(i) and U-thorite-(ii) to the line of theoretical A/B = 1/1 ratio.

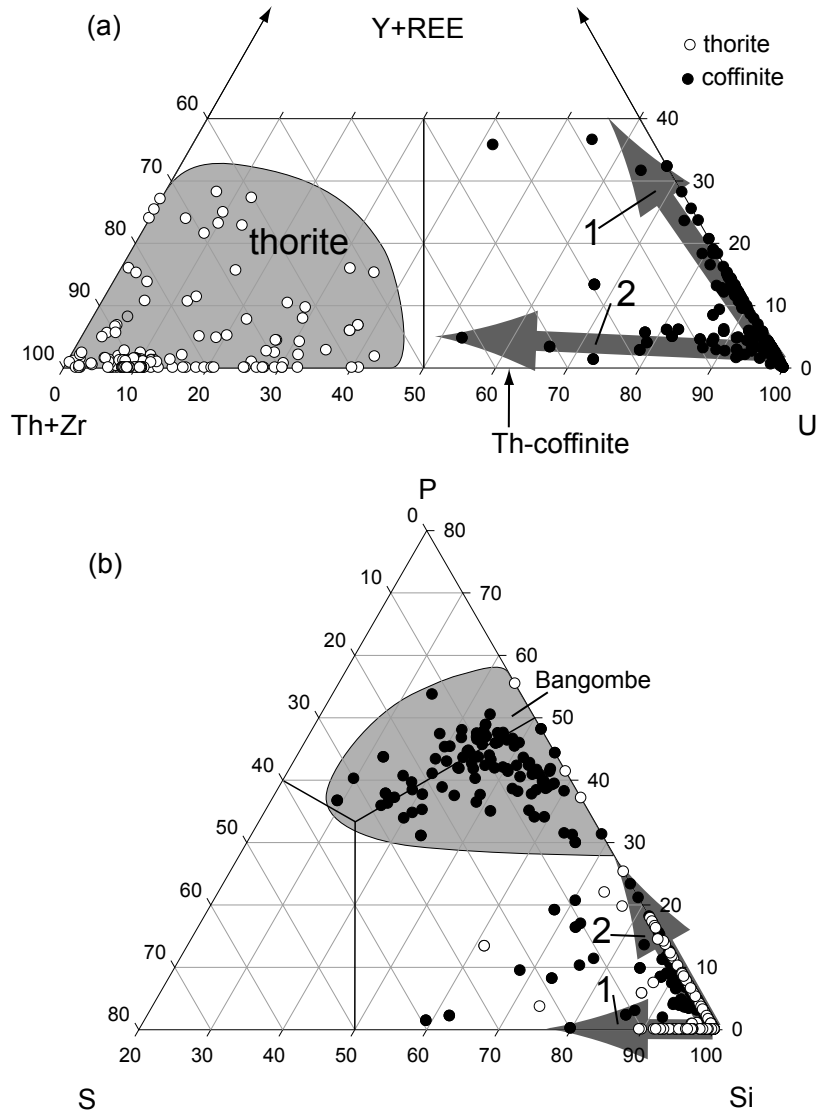


FIGURE 5. Compositions of U-thorite-(i), U-thorite-(ii), and Th-coffinite plotted on ternary diagrams. **(a)** (Th+Zr)-U-(Y+REE) and **(b)** S-Si-P. **(a)** Note that the shaded area indicates mixed compositions of thorite, whereas the two shaded arrows (1 and 2) mark trends of coffinite analyses along U-(Y+REE) and U-(Th+Zr) joins, respectively; (analyses of thorite >50 mol% of the end-member only). **(b)** Note that there are two trends of thorite: (1) along Si-S join; analyses of U-thorite from Madagascar; and (2) along the Si-P join (literature analyses; see references on Fig. 4). Coffinite analyses cluster in two areas of the Si-corner and around the boundary of 50/50 Si/P. The shaded area represents coffinite-xenotime end-members for P-coffinite from Bangombé (analyses after Deditius et al. 2009, and references therein).

incorporates Y+REE or Th without formation of mixed solid solutions (Fig. 5a). Two compositional trends are recognized for coffinite and are illustrated on Figure 5a: (1) represents substitution of Y+REE for U [up to 36.5 mol% of xenotime in coffinite from Ririvai (Pointer et al. 1988)], with most of the analyses plotting with <30 mol% xenotime; high contents of Y+REE were found in P-coffinite from Bangombé (Deditius et al. 2009; and references therein); and (2) represents isovalent substitution of Th for U (up to 42.2 mol% of thorite).

Figure 5b illustrates the distribution of thorite and coffinite analyses with respect to B-site cations in Si-P-S space. In this case, thorite forms two well-defined trends. The first, defined by the arrow along the Si-S join (indicated by U-thorite from

Madagascar) suggests that thorite may accumulate up to 10 mol% of $A^{2+}SO_4$ end-member. However, the combination of HRTEM observations and EMPA reveal that S-rich portion occurs in amorphous U-thorite-(i) (Figs. 2d and 3a). Consequently, it is not a true solid solution, but most likely S accumulates in the amorphous areas of U-thorite-(i) and U-thorite-(ii). The second trend extends along Si-P join. The highest amount of P has been reported by Johan and Johan (2005) as 55 mol% of xenotime, in thorite from Cínovec. However, the majority of the analyses cluster below 20 mol% xenotime (Fig. 5b). The coffinite analyses cluster in two areas. One is close to the Si corner; and the other is located in the broad area around 50/50 Si/P ratio, for P-coffinite from Bangombé as discussed in detail by Deditius et al. (2009).

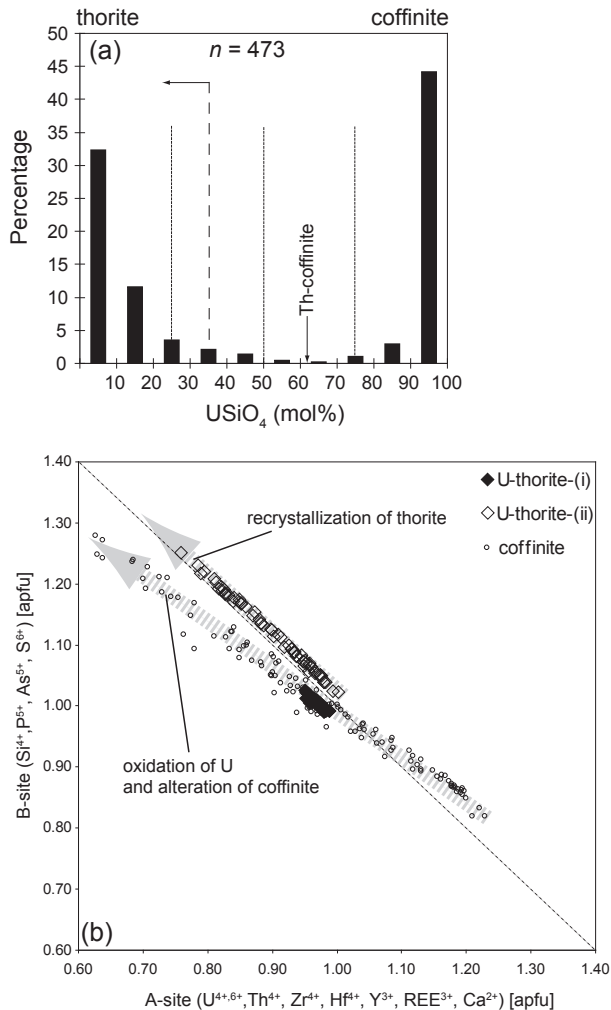


FIGURE 6. (a) Histogram of EMPA of thorite and coffinite presented in this work and reported by Förster (2006), Deditius et al. (2008, 2009), and references therein. Note that there is a bimodal distribution of U (as mol% of USiO_4) in the thorite-coffinite solid solution. The dotted lines mark intermediate compositions reported by Fuchs and Gebert (1958); the dashed line with an arrow indicates the maximum U solubility in thorite after Mumpton and Roy (1961). Note that the composition of nanoparticulate Th-coffinite plots in the range where only three analyses have been reported. (b) Comparison between total A-site and total B-site occupancy for U-thorite-(i) and U-thorite-(ii), and coffinite (analyses after Deditius et al. 2008). Two trends are shown; one represents the recrystallization of U-thorite along the line of theoretical A/B = 1/1 ratio; the other is related to the alteration of coffinite under oxidizing conditions, which deviates from the line of 1/1 ratio due to U-loss and increase in the Si concentration.

Chemical analyses of thorite and coffinite shown in Figure 6a document a strong, bimodal, and asymmetric distribution. More U is incorporated into thorite than Th in coffinite. Only three analyses plot within the range of 50–80 mol% USiO_4 . These analyses represent uranothorite from Witwatersrand and Ririwai (Pointer et al. 1988; Smits 1989). One might assume that the rarity of intermediate compositions may indicate a miscibility gap between thorite and coffinite. However, the range

of compositions from 50–80 mol% USiO_4 coincide with the measured Th/U ratio of 0.6 in the nanoparticulate Th-coffinite, $(\text{U}_{0.625}\text{Th}_{0.375})\text{SiO}_4$ (Fig. 3), which may be abundant in the U-thorite of similar U-content (<10 mol% USiO_4). Th-coffinite was not found in U-thorite in the Harding pegmatite (0.1–22 mol% USiO_4), but this sample contained V-rich thorite (Lumpkin and Chakoumakos 1988), whose properties may be different from pure orthosilicates. Similar variations of UO_2 content (1.8–9.5 wt%) in thorite were reported by Förster et al. (2000). Nanoscale analyses were not performed, but the authors noted characteristic patchy textures in thorite present in the analyzed samples, which may be indicative for nanoparticulate coffinite and/or actinide dioxides or orthosilicates (as in Fig. 1d). For example, a patchy texture in U-thorite was documented by Johan and Johan (2005). They showed that the euhedral crystals of U-thorite contain U-rich inclusions, as small as 1 μm , and concluded that the high concentrations of UO_2 (26.31 wt% or 34.4 mol% USiO_4) are in excess of the possible solubility limit reported by Mumpton and Roy (1961). Therefore, EMPA and HRTEM observations indicate that intermediate compositions of thorite-coffinite solid solution form nanoparticles as small as 4 nm. The observed nanoparticulate size of the intermediate solid-solution compositions may indicate their relatively lower thermodynamic stability than the bulk compositions (Navrotsky 2001). Thus, it is suggested that an increase in the U-content in thorite may cause a decrease in crystal size. In addition, formation of nanodomains of different composition was demonstrated in computational simulations where the thermodynamic stability of a 50/50 mixture of thorite and coffinite was examined (Ferriss et al. 2010).

Amorphization of (Th,U)-orthosilicates

The metamict state of U-thorite-(i), and the partial amorphization of U-thorite-(ii) observed in this study resulted from the accumulation of radiation damage from Th and U α -decay events. Although the exact location of the analyzed samples of U-thorite from Madagascar is not known, the calculated chemical ages of U-thorite reflect the general geological history of the island. The calculated ages of U-thorite-(i) that range from 2.1–1.9 and 1.8–1.6 Ga reflecting igneous and/or metamorphic activity have been reported from detrital zircon and monazite (e.g., Paquette and Nédélec 1998; Collins 2006; Tucker et al. 2011). The 1.6–0.5 Ga ages from crystalline U-thorite-(ii) with significant Pb-loss are most likely the result of fluid-induced recrystallization of amorphous U-thorite-(i). The youngest date (0.57 Ga) corresponds to the reported age of extensive magmatism and hydrothermal activity in Madagascar (Paquette and Nédélec 1998). This age was assumed in this study for the formation of U-thorite-(ii) and Th-coffinite.

The calculated maximal doses for U-thorite-(i) ($1.6\text{--}1.8 \times 10^{18}$ α -decay events/mg) are in the range of doses calculated for P-coffinite from the natural fission reactor in Bangombé (Gabon) (Deditius et al. 2009). However, no crystalline relicts have been found in U-thorite-(i) (Fig. 3a), which most probably reflects its higher energy for recrystallization (Lian et al. 2009) and/or an older age. The cumulative dose calculated for U-thorite-(ii) is slightly lower than the dose of $4\text{--}12 \times 10^{17}$ α -decay events/mg found in U-thorite from Harding pegmatite (Lumpkin and Chakoumakos 1988). In both cases, substantial crystallinity in

U-thorite is preserved. Similar orders of magnitude of dose were found in Th-coffinite, however no amorphization was noted, which suggests that coffinite remains crystalline whereas thorite experiences significant amorphization under similar conditions.

The lack of thorianite in the analyzed samples is consistent with thermodynamic and experimental data on the transformation of amorphized thorite (e.g., Meldrum et al. 1998; Lian et al. 2009; and references therein). The transformation of ThSiO_4 to $\text{ThO}_2+\text{SiO}_2$ requires high-temperature conditions (2250 K), which were not experienced by the analyzed samples. On the contrary, phase decomposition of USiO_4 to UO_2+SiO_2 for natural and synthetic coffinite occurs under lower temperature conditions (>673 and 573 K, respectively) (Lian et al. 2009). The lack of uraninite in the analyzed samples suggests that Th-coffinite formed at temperatures lower than 573 K. However, the coffinite accumulated significant amounts of Th with a Th/U ~0.6. It is suggested that Th in coffinite may have stabilized it to higher temperatures, thus preventing phase decomposition and transformation to the mixture of UO_2 and SiO_2 , as noted for the pure U-Si-O system (Lian et al. 2009). On the contrary, the high content of coffinite end-member (0.625 mol% of USiO_4) could be responsible for much lower activation energies for irradiation-enhanced recrystallization. Lian et al. (2009) reported a value of 0.28 (eV) for synthetic coffinite, which is significantly lower than the values of thorite, zircon, and hafnon (>3.0) (Meldrum et al. 1998).

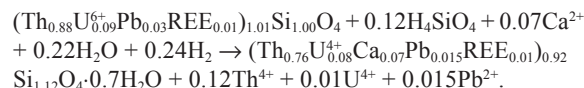
The distortion of single crystals of U-thorite-(ii) (Fig. 3) observed herein is similar to the reported formation of low-angle grain boundaries in zircon during crystalline-to-amorphous transition (Murakami et al. 1991), which suggests dynamic recrystallization and amorphization of U-thorite-(ii). Crystals of Th-coffinite are either well-oriented parallel to (001) lattice fringes or occur as random aggregates (Fig. 3f). To the best of our knowledge this is the first report of an oriented aggregate of nanoparticulate Th-coffinite similar to that observed in some minerals and synthetic compounds (Banfield et al. 2000; Banfield and Zhang 2001, and references therein). In addition, the lack of TEM-visible amorphization of Th-coffinite may be the result of its nanoparticulate size; i.e., annihilation of defects at grain boundaries (e.g., Zhang et al. 2009; Bai et al. 2010).

Alteration of U-thorite

Alteration of U-thorite under reducing and oxidizing conditions is poorly understood. Under oxidizing conditions U-thorite is transformed into uranophane, $\text{Ca}(\text{UO}_2)_2(\text{SiO}_3\text{OH})_2 \cdot 5\text{H}_2\text{O}$ (Abd El-Naby 2009) from the oxidation of U^{4+} to U^{6+} , whereas Th remains as the Th^{4+} species. In spite of the lack of precise locations for the U-thorite samples from Madagascar, the U-thorite–garnet–apatite–(CaF)–titanite–zircon mineral assemblage (Fig. 1) is indicative of crystalline rock, which is most likely magmatic-hydrothermal in origin. The ~1 cm size of the investigated U-thorite-(i) crystals, agrees relatively well with the large (hundreds of micrometers), single crystals of thorite formed under higher temperature conditions, ($T=400\text{--}600\text{ }^\circ\text{C}$) (e.g., Johan and Johan 2005). Under low-temperature conditions of sedimentary/diagenetic settings, microcrystalline thorite and/or coffinite precipitate (e.g., Smits 1989). Goldhaber et al. (1987) estimated that coffinite forms in sedimentary rocks

between 80 and 140 °C. The (Th,U)-orthosilicates at Ririwai most probably formed at $T < 260\text{ }^\circ\text{C}$, conditions under which U and Th were still mobile (Pointer et al. 1988). Experimental studies also confirm the formation of nanoparticulate coffinite and U^{4+} -silicates under lower temperature conditions of 180 °C (Amme et al. 2005) and 250 °C (Poiteau et al. 2009). The HRTEM observations document the nano-size of Th-coffinite and nano- to microcrystalline size of U-thorite-(ii) (Fig. 3). Consequently, it is suggested that the alteration processes and formation of secondary U-thorite-(ii) and Th-coffinite occurred under low-temperature conditions most probably at $T < 250\text{ }^\circ\text{C}$. In the analyzed samples, U-thorite-(ii) formed as a result of recrystallization of U-thorite-(i). However, the aggregates of Th-coffinite NPs are not associated with U-thorite-(i), but instead are attached to the U-thorite-(ii), which suggests that they precipitated directly from (U,Th)-rich solutions as a result of local supersaturation. In addition, there is no associated uraninite, which is often reported as the parent mineral to the subsequently formed coffinite (e.g., Janeczek and Ewing 1992a, 1992b). This is the case of Th-rich coffinite from the Witwatersrand reefs, where it formed as a result of interactions between Si-rich fluids and detrital uraninite. The higher-Th content in this particular coffinite was explained by partial removal of U and decoupled behavior of U and Th during alteration. The secondary Th-depleted coffinite (<5.9 wt% ThO_2) and uraninite from West Rand are suggested to have formed under reducing conditions of supergene environment (Smits 1989).

The observed alteration of U-thorite-(i) to U-thorite-(ii) resulted in the liberation of Th, U, and Pb, which is documented by the formation of U-thorite in the fractures of associated apatite and garnet at a maximum distance of 300 μm from the original grain (Fig. 1e). The loss of radiogenic Pb during thorite recrystallization was found by Lumpkin and Chakoumakos (1988), who reported PbS as the sink for lead. In the present example, it is assumed that 1 mole of U-thorite-(i) was altered to 1 mole of U-thorite-(ii). Consequently, the alteration reaction is as follows



Based on the spectroscopic studies by Farges and Calas (1991), the oxidation state of U in the amorphous U-thorite-(i) is assumed to be 6+. The average calculated content of H_2O , with a possible minor contribution from OH^- species (Fig. 2f) in U-thorite-(ii) is 4.4 wt%, or about 0.7 molecules of H_2O per formula unit. The calculated amount of 0.24 H_2 on the left side of the reaction indicates reducing conditions during alteration rather than molecular hydrogen in the altering fluid. The lack of uranyl minerals also suggests reducing conditions during alteration (Fig. 1). This reaction shows about an order of magnitude higher loss of Th than U from U-thorite that was subsequently sequestered by the formation of U-thorite-(ii) and Th-coffinite (Fig. 1e).

The observed patchy-like and collomorph textures in U-thorite-(i) (Figs. 1c and 1d) closely resemble the textures reported for U-thorite from other localities and the textures

noted above in hydrothermally altered zircon (e.g., Förster et al. 2000; Geisler et al. 2007); these textures are characterized by well-developed corrosion rinds at the grain boundaries between the parent phase and the product phase. Fracturing is due to the volume differences between the amorphous substrate and recrystallized products (e.g., Lumpkin 2001; Geisler et al. 2007). In addition, the alteration of orthosilicates is often associated with mobilization of liberated components, which results in the precipitation of different end-members of the orthosilicate (e.g., Geisler et al. 2007). Geisler et al. (2004) proposed that the recrystallization process of collomorphic zircon is due to diffusion of hydrogen, most likely in the form of molecular H₂O. Their model suggests repetitive generation of H-flux formed by the recrystallization of zircon and H-rejection from the zircon structure. As a result, ZrO₂ and amorphous SiO₂ are formed. In the present study no ThO₂ was found, for the reasons discussed in the previous section, but amorphous areas were observed (Figs. 3c–3d). The speciation of U in metamict U-thorite-(i) is most probably U⁶⁺, as reported by Farges and Calas (1991) in metamict U-thorite. We suggest that the oxidation of U from U⁴⁺ to U⁶⁺ occurred after formation of U-thorite; i.e., amorphization. Consequently, the presence of Th-coffinite (Figs. 3e–3f), a mineral unstable under oxidizing conditions (Deditius et al. 2008), suggests that U⁶⁺ was subsequently reduced to U⁴⁺ during its formation. Thus, it is suggested that hydrogen might be the reducing agent for the U⁶⁺-species liberated from U-thorite-(i).

Uranium and Th are characterized by decoupled geochemical behavior due to the oxidation of U⁴⁺ to U⁶⁺ and the stable speciation of Th⁴⁺ (e.g., Hazen et al. 2009). Decoupled behavior of U and Th during alteration of U-thorite is also noted in the specimens in this study, as indicated on the diagram that displays the sums of calculated occupancy of A and B sites in orthosilicates (Fig. 6b). Oxidation of U⁴⁺ in coffinite causes significant deviation of the U-trend, from the line of theoretical 1/1 ratio of A/B-site. This deviation is due to loss of cations from the A-site and an increase in the SiO₂ content (Deditius et al. 2008). The Th-trend follows the line of 1/1 ratio, and its extension toward the B-site is caused by an increase in SiO₂ content. The increase in SiO₂ content is likely due to SiO₂ accumulation in the amorphous areas (Fig. 3), as reported for other orthosilicates (e.g., Meldrum et al. 1998).

HRTEM and AEM analyses suggest that stability of coffinite relative to the mixture of UO₂+SiO₂ is extended if the other tetravalent actinides such as Th, Pu, Am, Cm substitutes for U in the coffinite structure. This may be due to the nanosize of the Th-coffinite and nanoparticulate, synthetic coffinite (Poiteau et al. 2009). Formation of Th-coffinite NPs during recrystallization of U-thorite under Si-rich, reducing conditions, suggests mixture of nanoparticulate phases with an intermediate composition in solid solutions of actinide-bearing orthosilicates (Th,Pu,U,Np)₄+SiO₄.

ACKNOWLEDGMENTS

The authors are grateful to Carl Henderson for help with electron microprobe analyses conducted at the Electron Microbeam Analysis Laboratory (EMAL) of the University of Michigan. The authors are also indebted to J. Janeczek and H. Hidaka for comments that improved the manuscript. This work was completed with support from the Materials Science of Actinides Center, an Energy Frontier Research Center funded by the U.S. Department of Energy, Office of Science, Office of Basic Energy Sciences under Award Number DE-SC0001089.

REFERENCES CITED

- Abd El-Naby, H.H. (2009) High and low temperature alteration of uranium and thorium minerals, Um Ara granites, south Eastern Desert, Egypt. *Ore Geology Reviews*, 35, 436–446.
- Amme, M., Wiss, T., Thiele, H., Boulet, P., and Lang, H. (2005) Uranium secondary phase formation during anoxic hydrothermal leaching processes of UO₂ nuclear fuel. *Journal of Nuclear Materials*, 341, 209–223.
- Bai, X.-M., Voter, A.F., Hoagland, R.G., Nastasi, M., and Uberuaga, B.P. (2010) Efficient annealing of radiation damage grain boundaries via interstitial emission. *Science*, 327, 1631–1634.
- Banfield, J.F. and Zhang, H. (2001) Nanoparticles in the environment. In J.F. Banfield and A. Navrotsky, Eds., *Nanoparticles and the Environment*, 44, p. 1–58. *Reviews in Mineralogy and Geochemistry*, Mineralogical Society of America, Chantilly, Virginia.
- Banfield, J.F., Welch, S.A., Zhang, H., Ebert, T.T., and Penn, R.L. (2000) Aggregation-based crystal growth and microstructure development in natural iron oxyhydroxide biomineralization products. *Science*, 289, 751–754.
- Berger, A., Gnos, E., Janots, E., Fernandez, A., and Giese, J. (2008) Formation and composition of rhabdophane, bastnäsite and hydrated thorium minerals during alteration: Implications for geochronology and low-temperature processes. *Chemical Geology*, 254, 238–248.
- Bowles, J.F.W. (1990) Age dating of individual grains of uraninite in rocks from electron microprobe analyses. *Chemical Geology*, 83, 47–53.
- Breiter, K., Čopjakova, R., and Skoda, R. (2009) The involvement of F, CO₂, and As in the alteration of Zr-Th-REE-bearing accessory minerals in the Hora Sväté Kateřiny A-type granite, Czech Republic. *Canadian Mineralogist*, 47, 1375–1398.
- Burns, P. (1999) The Crystal Chemistry of Uranium. In P.C. Burns and R.J. Finch, Eds., *Uranium: Mineralogy, Geochemistry and the Environment*, 38, p. 23–90. *Reviews in Mineralogy and Geochemistry*, Mineralogical Society of America, Chantilly, Virginia.
- Collins, A.S. (2006) Madagascar and the amalgamation of Central Gondwana. *Gondwana Research*, 9, 3–16.
- Deditius, A.P., Utsunomiya, S., and Ewing, R.C. (2008) The chemical stability of coffinite, USiO₄·nH₂O, 0 < n < 2, associated with organic matter: A case study from Grants uranium region, New Mexico, USA. *Chemical Geology*, 251, 33–49.
- Deditius, A.P., Utsunomiya, S., Wall, M.A., Poiteau, V., and Ewing, R.C. (2009) Crystal chemistry and radiation-induced amorphization of P-coffinite from the natural fission reactor at Bangombé, Gabon. *American Mineralogist*, 94, 827–836.
- Deditius, A.P., Utsunomiya, S., Poiteau, V., and Ewing, R.C. (2010) Precipitation and alteration of P-coffinite (USiO₄·nH₂O) in the presence of apatite. *European Journal of Mineralogy*, 22, 75–88.
- Ewing, R.C., Meldrum, A., Wang, L., and Wang, S. (2000) Radiation-induced amorphization. In S.A.T. Redfern and M.A. Carpenter, Eds., *Transformation Processes in Minerals*, 39, p. 319–361. *Reviews in Mineralogy and Geochemistry*, Mineralogical Society of America, Chantilly, Virginia.
- Farges, F. and Calas, G. (1991) Structural analysis of radiation damage in zircon and thorite: An X-ray absorption spectroscopic study. *American Mineralogist*, 76, 60–73.
- Ferriss, E.D.A., Ewing, R.C., and Becker, U. (2010) Simulations of thermodynamic mixing properties of actinide-containing zircon solid solutions. *American Mineralogist*, 95, 229–241.
- Finch, R.J. and Hanchar, J.M. (2003) Structure and chemistry of zircon and zircon group minerals. In J.M. Hanchar and P.W.O. Hoskin, Eds., *Zircon*, 53, p. 1–26. *Reviews in Mineralogy and Geochemistry*, Mineralogical Society of America, Chantilly, Virginia.
- Förster, H.-J. (2006) Composition and origin of intermediate solid solutions in the system thorite-xenotime-zircon-coffinite. *Lithos*, 88, 35–55.
- Förster, H.-J., Harlov, D.E., and Milke, R. (2000) Composition and Th-U and Pb total ages of huttonite and thorite from Gillespie's Beach, South Island, New Zealand. *Canadian Mineralogist*, 38, 675–684.
- Fuchs, L.H. and Gebert, E. (1958) X-ray studies of synthetic coffinite, thorite and uranorthites. *American Mineralogist*, 43, 243–248.
- Fuchs, L.H. and Hoekstra, H.R. (1959) The preparation and properties of uranium (IV) silicate. *The American Mineralogist*, 44, 1057–1063.
- Geisler, T., Seydoux-Guillaume, A.-M., Wiedenbeck, M., Wirth, R., Berndt, J., Zhang, M., Mihailova, B., Putnis, A., Salje, E.K.H., and Schlüter, J. (2004) Periodic precipitation pattern formation in hydrothermally treated metamict zircon. *American Mineralogist*, 89, 1341–1347.
- Geisler, T., Schaltegger, U., and Tomaschek, F. (2007) Re-equilibration of zircon in aqueous fluids and melts. *Elements*, 3, 43–50.
- Goldhaber, M.B., Hemingway, B.S., Mohagheghi, A., Reynolds, R.L., and Northrop, H.R. (1987) Origin of coffinite in sedimentary rocks by a sequential adsorption-reduction mechanism. *Bulletin de Minéralogie*, 110, 131–144.
- Grambow, B. and Giffaut, E. (2006) Coupling of chemical processes in the near field. *Materials Research Society Symposium Proceedings*, 932, 55–66.
- Hansley, P.L. and Fitzpatrick, J.J. (1989) Compositional and crystallographic data

- on REE-bearing coffinite from the Grants uranium region, northwestern New Mexico. *American Mineralogist*, 74, 263–270.
- Hazen, R.M., Ewing, R.C., and Sverjensky, D.A. (2009) Evolution of uranium and thorium minerals. *American Mineralogist*, 94, 1293–1311.
- Janeček, J. (1991) Composition and origin of coffinite from Jachymov, Czechoslovakia. *Neues Jahrbuch für Mineralogie*, 9, 385–395.
- (1999) Mineralogy and geochemistry of natural fission reactors in Gabon. In P.C. Burns and B. Finch, Eds., *Uranium: Mineralogy, Geochemistry and the Environment*, 38, p. 323–392. Reviews in Mineralogy and Geochemistry, Mineralogical Society of America, Chantilly, Virginia.
- Janeček, J. and Ewing, R.C. (1992a) Coffinitization—a mechanism for the alteration of UO_2 under reducing conditions. *Materials Research Society Symposium Proceedings*, 257, 497–504.
- (1992b) Dissolution and alteration of uraninite under reducing conditions. *Journal of Nuclear Materials*, 190, 157–173.
- Johan, Z. and Johan, V. (2005) Accessory minerals of the Cínovec (Zinnwald) granite cupola, Czech Republic: indicators of petrogenetic evolution. *Mineralogy and Petrology*, 83, 11–150.
- Kamineni, D.C. and Lemire, R.J. (1991) Thorite in fault zones of a granitic pluton, Atikokan, Canada: Implications for nuclear fuel waste disposal. *Chemical Geology*, 90, 133–143.
- Lian, J., Zhang, J.M., Pointeau, V., Zhang, F.X., Lang, M., Lu, F.Y., Poinssot, C., and Ewing, R.C. (2009) Response of synthetic coffinite to energetic ion beam irradiation. *Journal of Nuclear Materials*, 393, 481–486.
- Lumpkin, G.R. (2001) Alpha-decay damage and aqueous durability of actinide host phases in natural systems. *Journal of Nuclear Materials*, 289, 136–166.
- Lumpkin, G.R. and Chakoumakos, B.C. (1988) Chemistry and radiation effects in thorite-group of minerals from the Harding pegmatite, Taos, County, New Mexico. *American Mineralogist*, 73, 1405–1419.
- Meldrum, A., Zinkle, S.J., Boatner, L.A., and Ewing, R.C. (1998) A transient liquid-like phase in the displacement cascades of zircon, hafnium and thorite. *Nature*, 395, 56–58.
- Meldrum, A., Boatner, L.A., and Ewing, R.C. (2000) A comparison of radiation effects in crystalline ABO_4 -type phosphates and silicates. *Mineralogical Magazine*, 64, 185–194.
- Mumpton, F.A. and Roy, R. (1961) Hydrothermal stability of the zircon-thorite group. *Geochimica et Cosmochimica Acta*, 21, 217–238.
- Murakami, T., Chakoumakos, B.C., Ewing, R.C., Lumpkin, G.R., and Weber, W.J. (1991) Alpha-decay event damage in zircon. *American Mineralogist*, 76, 1510–1532.
- Navrotsky, A. (2001) Thermochemistry of nanomaterials. In J.F. Banfield and A. Navrotsky, Eds., *Nanoparticles and the Environment*, 44, p. 73–103. Reviews in Mineralogy and Geochemistry, Mineralogical Society of America, Chantilly, Virginia.
- Paquette, J.L. and Nédélec, A. (1998) A new insight into Pan-African tectonics in the East-West Gondwana collision zone by U-Pb zircon dating of granites from central Madagascar. *Earth and Planetary Science Letters*, 155, 45–56.
- Pettke, T., Audétat, A., Schaltegger, U., and Heinrich, C.A. (2005) Magmatic-to-hydrothermal crystallization in the W-Sn mineralized Mole Granite (NSW, Australia) Part II: Evolving zircon and thorite trace element chemistry. *Chemical Geology*, 220, 191–213.
- Pointeau, V., Deditius, A.P., Miserque, F., Renock, D., Becker, U., Zhang, J., Clavier, N., Dacheoux, N., Poinssot, C., and Ewing, R.C. (2009) Synthesis and characterization of coffinite. *Journal of Nuclear Materials*, 393, 449–458.
- Pointer, C.M., Ashworth, J.R., and Ixer, R.A. (1988) The zircon-thorite mineral group in metasomatized granite, Ririwai, Nigeria. 1. Geochemistry and metastable solid solution of thorite and coffinite. *Mineralogy and Petrology*, 38, 245–262.
- Shannon, R.D. (1976) Revised effective ionic radii and systematic studies of interatomic distances in halides and chalcogenides. *Acta Crystallographica*, A32, 751–767.
- Smits, G. (1989) (U,Th)-bearing silicates in reefs of the Witwatersrand, South Africa. *Canadian Mineralogist*, 27, 643–655.
- Spear, J.A. (1982) The actinide orthosilicates. In P.H. Ribbe, Ed., *Orthosilicates*, 5, p. 113–135. Reviews in Mineralogy, Mineralogical Society of America, Chantilly, Virginia.
- Tucker, R.D., Roig, J.Y., Macey, P.H., Delor, C., Amelin, Y., Armstrong, R.A., Rabarimanana, M.H., and Ralison, A.V. (2011) A new geological framework for south-central Madagascar, and its relevance to the “out-of-Africa” hypothesis. *Precambrian Research*, 185, 10–130.
- Zhang, J.M., Lian, J., Fuentes, A.F., Zhang, F.X., Lang, M., Lu, F.Y., and Ewing, R.C. (2009) Enhanced radiation resistance of nanocrystalline pyrochlore $\text{Gd}_2(\text{Ti}_{0.65}\text{Zr}_{0.35})\text{O}_7$. *Applied Physics Letters*, 94, 243110.
- Žáček, V., Škoda, R., and Sulovský, P. (2009) U-Th-rich zircon, thorite and allanite-(Ce) as main carriers of radioactivity in the radioactive ultrapotassic melysyenite porphyry from the Šumava Mts., Moldanubian Zone, Czech Republic. *Journal of Geosciences*, 54, 343–354.

MANUSCRIPT RECEIVED JULY 15, 2011

MANUSCRIPT ACCEPTED NOVEMBER 22, 2011

MANUSCRIPT HANDLED BY AARON CELESTIAN